Journal of Chromatography A, 1433 (2016) 75–84

Contents lists available at ScienceDirect

Journal of Chromatography A

journal homepage: www.elsevier.com/locate/chroma

Detailed kinetic performance analysis of micromachined radially elongated pillar array columns for liquid chromatography

Manly Callewaert[a,b], Gert Desmet[a], Heidi Ottevaere[b], Wim De Malsche[a,*]

[a] Department of Chemical Engineering, Vrije Universiteit Brussel, Pleinlaan 2, 1050 Brussels, Belgium
[b] B-PHOT, Department of Applied Physics, Vrije Universiteit Brussel, Pleinlaan 2, 1050 Brussels, Belgium

ARTICLE INFO

Article history:
Received 18 September 2015
Received in revised form
17 December 2015
Accepted 18 December 2015
Available online 8 January 2016

Keywords:
Pillar array column
Column packing
Lab-on-a-chip
Microfluidics
Open tubular
Radially elongated pillar

ABSTRACT

The individual factors that determine the kinetic performance (B- and C-term band broadening and bed permeability K_v) of radially elongated pillar (REP) columns are studied. To this end, columns with REPs having 4 different aspect ratios (AR = 9, 12, 15, 20) were characterized experimentally and by means of numerical simulations. A tortuosity and retention based plate height equation was established, enabling a good global fit for all studied conditions. The B-term plate height contribution appears to decrease with a factor equaling the square of the flow path tortuosity τ. Going from AR = 12 to AR = 20 (τ = 5.7 and τ = 9.0 respectively), this resulted in a shift in plate height expressed in axial coordinates from H_{min} = 0.42 μm to H_{min} = 0.25 for non-retained conditions and from H = 0.77 μm to H = 0.57 μm for a component with k = 1.0. The obtained parameters were combined to predict optimal time-efficiency combinations for all possible channel lengths. This revealed an efficiency limit of $N = 10^7$ plates for a non-retained component and $N = 7–8 \times 10^6$ for k = 1 for a channel with an AR = 20, corresponding to a channel length of 2.5 m and a void time of 2.4 h.

1. Introduction

During the last decade, pillar array columns have been intensively studied in the context of liquid chromatography [1,2]. The sheer unlimited flexibility in terms of shape and spacing of the support structures is very attractive, as it quite straightforwardly allows to conceive configurations that are predicted to be superior on a theoretical basis. The ability to achieve perfect order is an important asset of the pillar array column format, which represents an alternative to other emerging column fabrication approaches, such as 2 photon polymerization [3] and colloidal crystals [4]

An established column format, the open tubular column (OTC), is since long considered as the best achievable column format. Due to the single flow path eddy dispersion is lacking and the undisturbed symmetrical flow configuration seems to provide the optimal flow configuration, when detection and loadability issues are neglected [5].

In a recent paper [6], we have postulated that the intrinsic band broadening experienced by the fluid in the tortuous flow-through pores running through a micro-pillar array column filled with radially elongated pillars (REPs) is identical to that experienced in open-tubular column with the same (flat-rectangular) cross-section as the trough-pores in the REP bed. This postulation was based on the fact that the velocity field established in the through-pores between the pillars (which runs along the *i*-coordinate indicated by the arrow added to Fig. 1a) in the REP column is perfectly equivalent to that in an OTC. A small deviation occurs at the turns and connection points in the REP column, but these only make up a small fraction of the total trajectory and can hence be neglected to a first extent.

We could also demonstrate mathematically that the number of theoretical plates (N_x) observed in the mean flow direction, i.e., along the *x*-axis, is the same as the number of plates one would observe along the internal *i*-coordinate describing the tortuous path followed by the fluid (N_i, see Fig. 1a for definition of *x*- and *i*-coordinate):

$$N_x = \frac{L_x^2}{\sigma_x^2} = \frac{L_i^2}{\sigma_i^2} = N_i \quad (1)$$

The physical meaning of Eq. (1) is that, regardless whether one measures the efficiency along the shortest distance (i.e., along the folded distance, or *x*-domain) or along the actual flow path (stretched distance, or *i*-domain), one gets the same efficiency, as it should be for a universally valid measure.

* Corresponding author.
E-mail address: wdemalsc@vub.ac.be (W. De Malsche).

http://dx.doi.org/10.1016/j.chroma.2015.12.086
0021-9673/

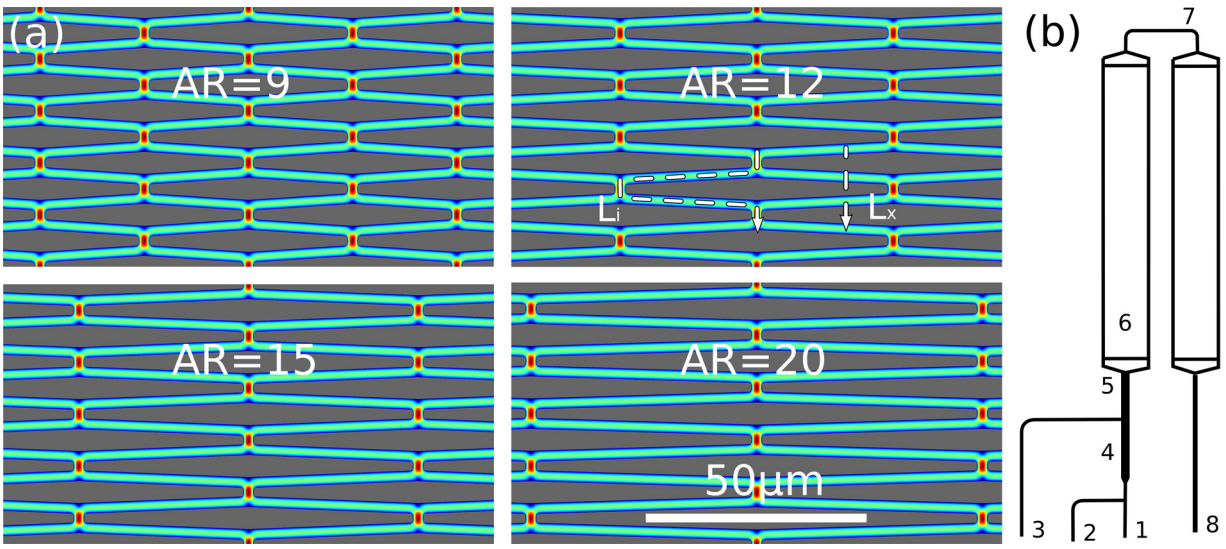

Fig. 1. (a) Schematic overview of the studied radially elongated pillar configurations with aspect ratio AR = 9, 12, 15 and 20 (channel spacing 2.3 μm). The colors correspond to the mobile phase velocity (increasing from dark blue to red). (b) Schematic overview of the channel layout containing the mobile phase inlet (1), the injection phase inlet (2), the injection phase outlet (3), the injection box (4), the distributor (5), the REP packing (6), a turn between both channel tracks (7) and the channel outlet (8). (For interpretation of the references to color in this figure legend, the reader is referred to the web version of this article.)

Also the time is independent of the selected measurement frame, such that:

$$t_x = \frac{L_x}{u_x}(1+k) = \frac{L_i}{u_i}(1+k) = t_i \tag{2}$$

with t_x and t_i the respective time required for a non-retained component to reach downstream position L_x, for which an effective length L_i has been passed, k the retention coefficient and u_x and u_i the axial and local velocity.

The key parameter linking the system variables and performance parameters measured in either the x-or i-direction is the tortuosity factor τ, defined as:

$$\tau = \frac{L_i}{L_x} = \frac{u_i}{u_x} \tag{3}$$

It is important to realize that this tortuosity factor also relates the band width (and the standard deviation σ) observed in the x- to that observed in the i-direction, because the tortuosity effect also squeezes the width of the bands when observed in the x-coordinate system with respect to that observed in i-direction:

$$W_x = \frac{W_i}{\tau} \text{ and} \sigma_x^2 = \frac{\sigma_i^2}{\tau^2} \tag{4}$$

As can easily be verified, Eqs. (3) and (4) provide the necessary relations to justify all transformations made in Eqs. (1) and (2). Combination of Eqs. (1) and (3) also readily shows that, despite the perfect similarity in band broadening and mass transfer properties, the plate height value H is not an invariant between the i- and x-coordinate system:

$$H_x \equiv \frac{\sigma_x^2}{L_x} = \frac{\sigma_i^2}{L_i}\frac{1}{\tau} = \frac{H_i}{\tau} \tag{5}$$

Eq. (5) implies that the plate height observed from the spatial band variance in a REP column will appear τ times smaller than in the corresponding system with straight-running throughpores. This shows that the plate height itself is not a relevant performance parameter when comparing systems with a strongly differing geometry. Instead, the number of plates per given time (=kinetic performance) is much better suited, as it does not depend on the considered coordinate system and is furthermore also practically much more relevant.

To understand the behavior observed in [6], we have investigated how the individual factors contributing to the kinetic performance of REP columns (B-term band broadening, C-term band broadening, bed permeability K_v) depend on the detailed geometry of the bed. This was done by comparing 4 different column geometries, all having the same external porosity (or similarly, packing density) but filled with pillars with a different aspect ratio (ARs, see Fig. 1). The AR is defined as the ratio of the lateral and the axial dimension. Four ARs are considered; AR = 9, AR = 12, AR = 15, AR = 20. The B-term band broadening is measured separately using so-called peak parking [7,8]. The obtained experimental results are subsequently compared to existing theoretical models. Subsequently, the information on the band broadening is combined with column permeability data obtained via numerical modeling to determine the over-all kinetic performance of the system. This is done using a kinetic plot, plotting the optimal combination of time and efficiency that can be realized for all possible column lengths.

2. Experimental

2.1. Geometry and microfabrication

The geometry of the studied pillar arrays with different aspect ratios (9, 12, 15, 20) is depicted in Fig. 1a. The channel consisted of 2 channel tracks of 2 cm long connected by a low dispersion distributor-turn structure (see Fig. 1b) [9]. The pillar-array columns (inter-pillar distance 2.5 μm on mask) were patterned with photolithography (photoresist, Olin 907-12), and a dry etching step (Adixen AMS100DE, Alcatel Vacuum Technology, Culemborg, The Netherlands) of a 200 nm thick SiO_2 layer below. After that, mobile phase and sample supply channels were patterned and etched (130 μm deep). After removing the resist with oxygen plasma and nitric acid, the pillars were defined in the SiO_2 mask and subsequently Bosch etched to a depth of 18 μm deep. The silicon wafer was then anodically bonded to a Pyrex wafer (thickness 0.5 mm) with an EVG EV-501 wafer bonder (EV Group Inc., Schaerding, Austria). The chip was subsequently diced (100 μm deep) from both sides of the wafer, exposing the grooves wherein the interfacing capillaries fit (108 μm OD and 40 μm ID) after breaking the chip at the area of the dicing lines. Next, the capillaries were inserted and sealed with epoxy glue.